minerals

MDPI

Article

Paleopressure during Hydrocarbon Charging and Its Evolution in the Funing Formation of the Gaoyou Sag, Subei Basin, Eastern China

Chunquan Li [1,*], Shiyou Qian [2] and Yuancai Zheng [2]

[1] Department of Petroleum Geology, School of Earth Resources, China University of Geosciences, Wuhan 430074, China
[2] Exploration and Development Research Institute of Jiangsu Oilfield Company, SINOPEC, Yangzhou 225009, China; qiansy.jsyt@sinopec.com (S.Q.); zhengyc.jsyt@sinopec.com (Y.Z.)
* Correspondence: chunquanli@cug.edu.cn

Abstract: Abnormally high pressures are currently limited and locally developed in the Funing Formation of the Gaoyou Sag, Subei Basin, eastern China, but the paleopressure and its evolutionary history remain unclear. Based on the determination of hydrocarbon charging periods by performing systematic fluid inclusion analysis on sixteen core samples from the Funing Formation, thermodynamic modeling with fluid inclusion data was adopted to reconstruct the paleopressure and redisplay its evolutionary history throughout geological time. Results showed that the Funing Formation experienced two episodes of hydrocarbon charging periods. Episode 1 occurred with the charging of lower maturity oils in the period from 52.8 Ma to 49.5 Ma, which was recorded by yellow-fluorescing oil inclusions. Episode 2 happened with the charging of higher maturity oils in the period from 47.0 Ma to 37.0 Ma, which was characterized by blue-fluorescing oil inclusions. Each episode was an abnormally high-pressured hydrocarbon charging process. The pressure coefficient of Episode 1 reached as high as 1.44, while that of Episode 2 reached as high as 1.40. The current formation pressure is the evolutionary result of paleopressure after a process of rapid increasing and decreasing and slow increasing and is not as high as what it reached during the hydrocarbon charging periods. This work is valuable for the exploration of conventional clastic oil reservoirs and unconventional shale oils in the Funing Formation.

Keywords: fluid inclusion; hydrocarbon charging period; paleopressure reconstruction; thermodynamic modeling; Gaoyou Sag; Subei Basin

check for updates

Citation: Li, C.; Qian, S.; Zheng, Y. Paleopressure during Hydrocarbon Charging and Its Evolution in the Funing Formation of the Gaoyou Sag, Subei Basin, Eastern China. *Minerals* **2024**, *14*, 821. https://doi.org/10.3390/min14080821

Academic Editor: Thomas Gentzis

Received: 14 July 2024
Revised: 6 August 2024
Accepted: 12 August 2024
Published: 14 August 2024

Copyright: © 2024 by the authors. Licensee MDPI, Basel, Switzerland. This article is an open access article distributed under the terms and conditions of the Creative Commons Attribution (CC BY) license (https://creativecommons.org/licenses/by/4.0/).

1. Introduction

Formation pressure has been intensively studied in the exploration and exploitation of oil and gas in a sedimentary basin, with a particular focus on two aspects: current pressure and paleopressure [1–6]. The current pressure (present-day formation pressure), especially the current abnormal formation pressure, has a close relationship to the present distribution of oil and gas reservoirs [7], and the paleopressure (formation pressure at a certain geological time), from which the current pressure evolved, is of great significance for further understanding the hydrocarbon migration and accumulation mechanisms. The current pressure can be directly obtained through some borehole tests, such as the DST (Drill Stem Test) and RFT (Repeat Formation Test), or indirectly calculated with seismic or logging data [8,9], but the determination of paleopressure is not an easy task. Nonetheless, researchers have established forward and backward methods for obtaining paleopressure at any geological time, and basin modeling is the most popular one of such methods [10]. With the utilization of fluid inclusions in hydrocarbon exploration and exploitation, some *P-V-T* modeling methods to excavate paleopressure with fluid inclusions have been developed and some relative problems that need attention when using these methods have also been

fully discussed [11–14]. Many case studies have proved that the fluid inclusion technique can be economically and conveniently used to reconstruct the paleopressure and redisplay the whole evolution process from ancient to current times [15–17].

In the Funing Formation in the Gaoyou Sag of the Subei Basin, eastern China, it has been revealed in recent oil and gas exploration that abnormally high pressures are limitedly developed and locally distributed, but the evolutionary process, especially the paleopressure state during the hydrocarbon charging periods, is unclear. Therefore, this paper adopts a fluid inclusion technique to determine the hydrocarbon charging periods and reconstruct the evolution process of paleopressure so that some meaningful information can be established and used as an essential reference in further hydrocarbon exploration and exploitation in the study area.

2. Geological Setting

The Subei Basin, a petroliferous lacustrine basin with an area of approximately 3.5×10^4 km^2, is situated in eastern China (Figure 1a,b). It is bounded by the western margin of the Yellow Sea to the east, the Tanlu Fault to the west, the Binhai Uplift to the north, and the Tongyang Uplift to the south and is separated by the Jianhu Uplift within the basin into two depressions: the Yanfu Depression in the north and the Dongtai Depression in the south (Figure 1c). The Subei Basin developed in the Late Cretaceous [18,19] and deposited over 7000 m of sedimentary sequences, which are mainly composed of the upper Cretaceous Taizhou Formation (K_2t), the Paleocene Funing Formation (E_1f), the Eocene Dainan Formation (E_2d) and Sanduo Formation (E_2s), the Miocene–Pliocene Yancheng Formation (Ny), and the Pleistocene–Holocene Dongtai Formation (Qd) (Figure 2). During its evolution, the Subei Basin has undergone multiple tectonic stages [18,19]: (1) the rifting stage, which was interrupted by the late Paleocene Wubao event into stage I (K_2t-E_1f) and stage II (E_2d-E_2s); (2) the uplift stage, which was triggered by the Sanduo event, leading to prolonged exposure and erosion throughout the Oligocene after the period of E_2s; and (3) the post-rift subsidence stage (Ny-Qd) (Figure 2).

The Gaoyou Sag, occupying the central part of the Dongtai Depression, covers an area of 2670 km^2 (Figure 1c). As a semi-graben, the Gaoyou Sag is controlled by the southern fault zone, composed of the Zhen 1, Zhen 2, Wu 1, and Wu 2 faults (Figure 1d,e). These four major faults, combined with the Hanliu Fault, separate the Gaoyou Sag into three tectonic units: the southern fault terrace zone, the central sag zone, and the northern slope zone (Figure 1d,e). The Gaoyou Sag is the most oil-rich sag of the Subei Basin. Oil reservoirs in the sag occur mostly in the formations of E_2d and E_1f and are distributed around the major faults and within the northern slope zone (Figure 1d). The reservoir oils are mainly sourced from the formation of K_2t and E_1f [20,21]. Therefore, E_1f is not only the main source unit but also the main accumulation unit of oils. It is sub-divided into four members, namely E_1f_1, E_1f_2, E_1f_3, and E_1f_4, from the base upwards (Figure 2). The E_1f_2 and E_1f_4 were deposited in semi-deep and deep lakes, containing organic-rich grayish black mudstones, which made them the primary source rocks of conventional clastic reservoirs [22] and the main target of recent unconventional shale oil exploration [23], whereas the E_1f_1 and E_1f_3 were developed in delta environments, embracing sandstones, which made them the clastic reservoir rocks for conventional oil accumulation [24].

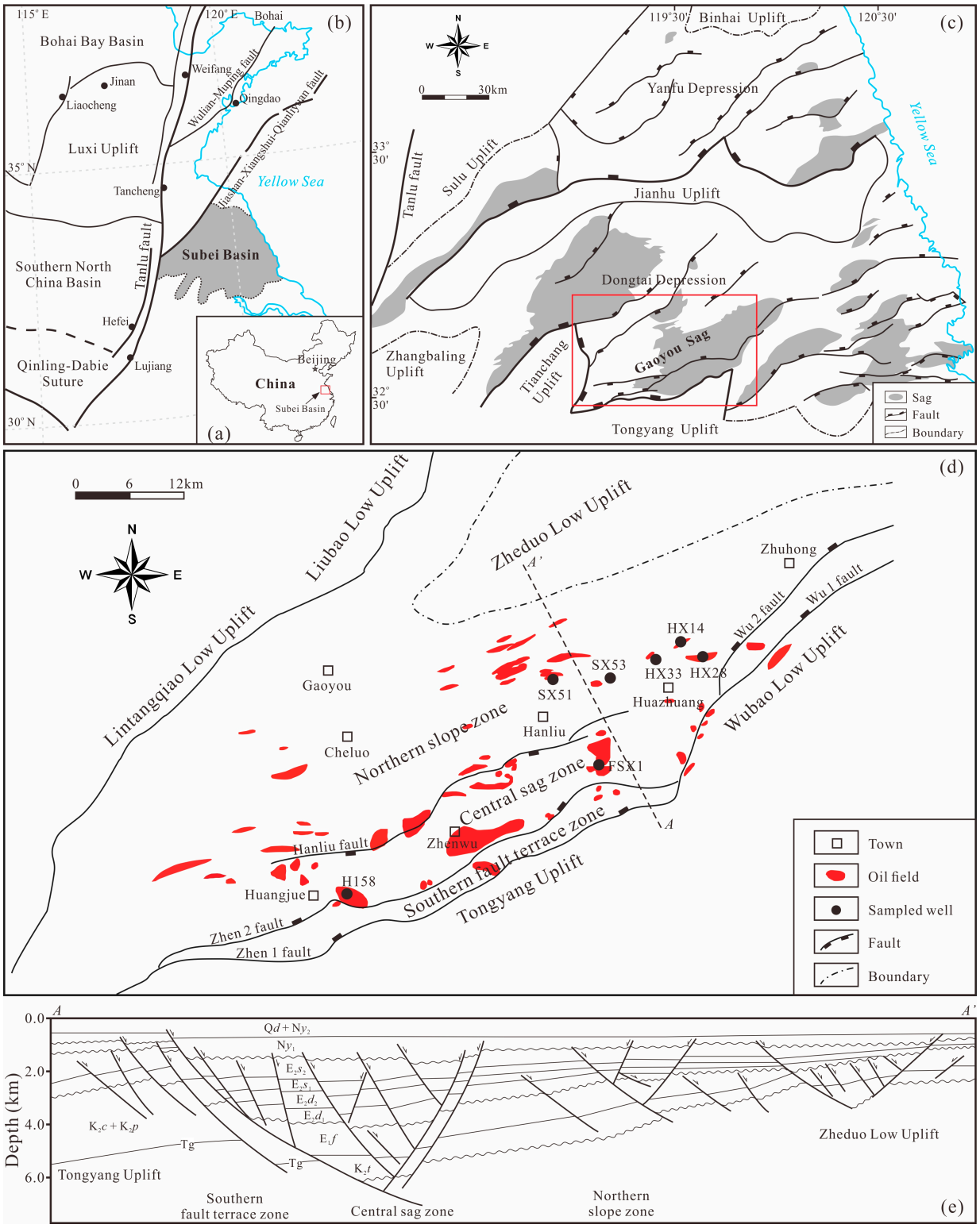


Figure 1. Geological maps of the study area: (**a**,**b**) The location of the Subei Basin in China; (**c**) the main structures in the Subei Basin and the location of the Gaoyou Sag (the red square); (**d**) tectonic sub-units in the Gaoyou Sag and the distribution of oil reservoirs and sampled wells; (**e**) the structural profile of the Gaoyou Sag along the AA′ section in (**d**).

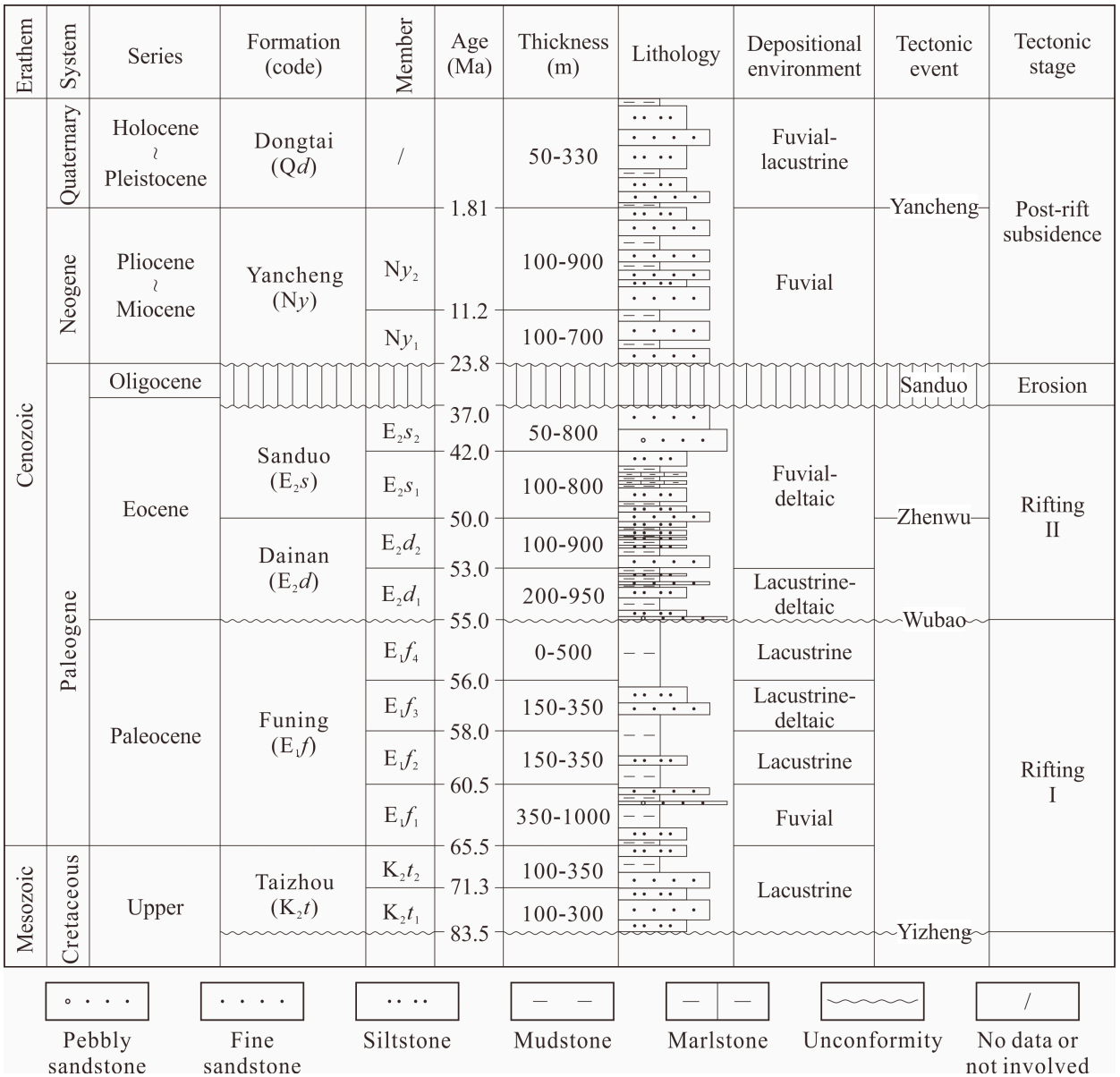


Figure 2. Stratigraphic column of the Gaoyou Sag showing detailed ages, depositional environments, tectonic events, and tectonic stages.

3. Samples and Methods

3.1. Samples

In this study, sixteen drilling core samples were collected from the Funing Formation of seven wells in the Gaoyou Sag (Table 1). Among these sampled wells, five are in the east part of the northern slope zone, and two are in the east and the west part, respectively, of the central sag zone (Figure 1d). The samples are mostly from E_1f_1 and E_1f_3, with eight and six samples, respectively, except for one from the E_1f_2 and one from the E_1f_4. Lithologically, ten samples are siltstone, two samples are fine sandstone, one sample is fine sandstone with a calcite vein, and three samples are mudstone with a calcite vein (Table 1). All samples were handled into double-polished thin sections for systematic analysis of fluid inclusions.

Table 1. Sample information and microspectrofluorimetric and microthermometric results of typical oil and coeval aqueous inclusions.

Well	Sample #	Depth (m)	Formation	Lithology	Fluorescence Color	λ_{max} (nm)	$Q_{650/500}$	Th_{oil} (°C)	Th_{aq} (°C)	Occurrence
SX51	1	2699.00	E_1f_3	Siltstone	Yellow	567.9	0.71	68.6	80.4	CTQG
					Blue	521.0	0.39	88.7	98.5	CTQG
SX53	2	3058.60	E_1f_1	Siltstone	Yellow	542.7	0.57	75.6	84.3	CWQG
	3	2854.85	E_1f_3	Siltstone	Yellow	542.2	0.64	95.6	106.5	CTQG
HX14	4	3143.30	E_1f_1	Siltstone	Yellow	545.0	0.72	62.6	72.6	CWQG
					Blue	520.1	0.44	98.6	108.5	CTQG
	5	3147.60	E_1f_1	Siltstone	Yellow	579.1	0.79	68.1	78.1	CTQG and CWQG
					Blue	523.3	0.42	100.4	112.3	CWQG
HX28	6	3265.89	E_1f_3	Siltstone	Blue	499.7	0.28	93.4	103.4	CTQG
	7	3268.00	E_1f_3	Siltstone	Yellow	543.1	0.60	87.8	97.8	CTQG
HX33	8	3201.75	E_1f_1	Siltstone	Yellow	543.1	0.78	93.4	103.5	CTQG and CWQG
	9	3208.90	E_1f_1	Siltstone	Yellow	541.8	0.56	91.3	100.2	CTQG
	10	3295.00	E_1f_1	Siltstone	Blue	504.3	0.30	98.4	108.4	CTQG
FSX1	11	3553.60	E_1f_3	Fine sandstone	Blue	490.2	0.27	109.8	119.2	CWQG
	12	3557.60	E_1f_3	Fine sandstone	Yellow	574.6	0.75	93.4	103.4	CWQG
					Blue	511.1	0.37	95.6	105.6	CTQG
	13	3845.30	E_1f_2	Mudstone with calcite vein	Blue	493.4	0.22	96.4	106.4	Calcite veins
	14	3949.00	E_1f_1	Mudstone with calcite vein	Blue	496.6	0.26	107.9	117.2	Calcite veins
	15	4046.50	E_1f_1	Fine sandstone with calcite vein	Blue	487.5	0.32	106.8	117.2	Calcite veins
H158	16	3162.20	E_1f_4	Mudstone with calcite vein	Yellow	549.9	0.66	101.9	111.9	Calcite veins
					Blue	517.0	0.33	129.1	139.1	Calcite veins

Notes: λ_{max}—wavelength of maximum intensity in a fluorescence spectrum; $Q_{650/500}$—ratio of the intensity at 650 nm to the intensity at 500 nm in a fluorescence spectrum; Th_{oil}—homogenization temperature of oil inclusion; Th_{aq}—homogenization temperature of coeval aqueous inclusion; CTQG—cracks through quartz grain; CWQG—cracks within quartz grain.

3.2. Methods

3.2.1. Petrography

All the double-polished thin sections were initially observed with a dual-channeled Nikon 80i microscope under transmitted (TR) light (Nikon Instruments Inc., Tokyo, Japan) to characterize fluid inclusions. Meanwhile, the same field view was also observed under ultraviolet (UV) light so that oil inclusions could be quickly distinguished from aqueous inclusions through their fluorescence behavior [25]. During this procedure, the fluid inclusion assemblage (FIA) principle [26] was strictly followed and common problems and pitfalls in fluid inclusion study [27] were sufficiently overcome to make sure the oil inclusions and their coeval aqueous inclusions were represented. Moreover, information such as occurrences, shapes, and sizes of the coeval oil and aqueous inclusions were recorded, as well as the fluorescence colors of oil inclusions recognized by the naked eye.

3.2.2. Fluorescence Microspectroscopy

Oil inclusions emit visible fluorescence in the range of 400–700 nm under UV light irradiation, and the fluorescence emission is recognized by the naked human eye as a color. To limit deviation in color recognition between persons, the fluorescence emission of oil inclusion was measured spectroscopically from 300 nm to 1000 nm by using an Ocean Optics Maya2000 Pro spectrometer (Ocean Insight, Orlando, FL, USA) coupled to the dual-channeled Nikon 80i microscope, which has a 100 W high-pressure mercury-vapor light source. Fluorescence spectra were collected through Yuanao software (Version 3.0) and quantified using the parameters λ_{max} (the wavelength of maximum intensity) and $Q_{650/500}$ (red/green, ratio of the intensity at 650 nm to the intensity at 500 nm) [25,28]. As fluorescence parameters, λ_{max} and $Q_{650/500}$ have been related to thermal maturity parameters of inclusion oils [28], which suggests that as the λ_{max} and $Q_{650/500}$ increases, the maturity decreases.

3.2.3. Microthermometry and Thermodynamic Modeling

Microthermometry was performed on coeval oil and aqueous inclusions to acquire their homogenization temperatures by using a Linkam THMS G600 (Linkam Scientific Instruments Ltd., Redhil, UK) heating/cooling stage mounted to the dual-channeled Nikon 80i microscope, which was equipped with a Nikon 100× long-working distance objective lens (Nikon Instruments Inc., Tokyo, Japan). The stage was calibrated with synthetic fluid inclusions and gave the results with a precision of 0.1 °C. When performing microthermometry, the heating rate was set as 10 °C/min during the initial stage of each heating-ramp and then reduced to 1 °C/min near the homogenization temperature till the final homogenization so that reliable homogenization temperatures could be obtained. Moreover, fluid inclusions (either oil or aqueous) experiencing post-entrapment changes, such as necking down, stretching, leakage, or refilling, were all excluded from microthermometry because they are non-representative [29].

Thermodynamic modeling with fluid inclusions was adopted to restore the inclusion trapping pressure, which stands for the paleopressure of the formation. With a series of trapping pressures excavated, the characteristics of paleopressure evolution could be reconstructed. VTflinc software was chosen to fulfill the thermodynamic modeling. It is the sister program of PVTSim and is commonly used to perform iterative series of calculations to reconstruct the hydrocarbon phase envelope and isochore based on the *V*(volume)-*T*(temperature)-*x*(composition) properties of hydrocarbon [15,16,30]. The main inputs include the homogenization temperatures of oil inclusion and its coeval aqueous inclusion, the composition of inclusion oil, and the bubble volume of oil inclusion at room temperature. Homogenization temperatures come from microthermometry. The bubble volume of oil inclusion was measured by using a confocal laser scanning microscope [12], and a Leica TCS SPE confocal system was used in this work. The composition of inclusion oil can be optimized through the flash method by VTflinc based on the initial input of current reservoir oil composition, homogenization temperature, and bubble volume data from coeval oil and aqueous inclusions. The result of thermodynamic modeling comes out as a *P-T* phase diagram showing the trapping pressure of inclusion.

4. Results

4.1. Petrography

Fluid inclusions in the Funing Formation of the Gaoyou Sag were commonly trapped in calcite veins of mudstone and along cracks within or through the quartz grains of sandstone (Figure 3). Oil inclusions fluorescing yellow and blue were observed, accompanying non-fluorescing aqueous inclusions. Petrographically, these coeval oil and aqueous inclusions are dominantly secondary inclusions and record information on hydrocarbon activities. Hence, they can be used to unveil the processes of hydrocarbon generation, migration, and accumulation.

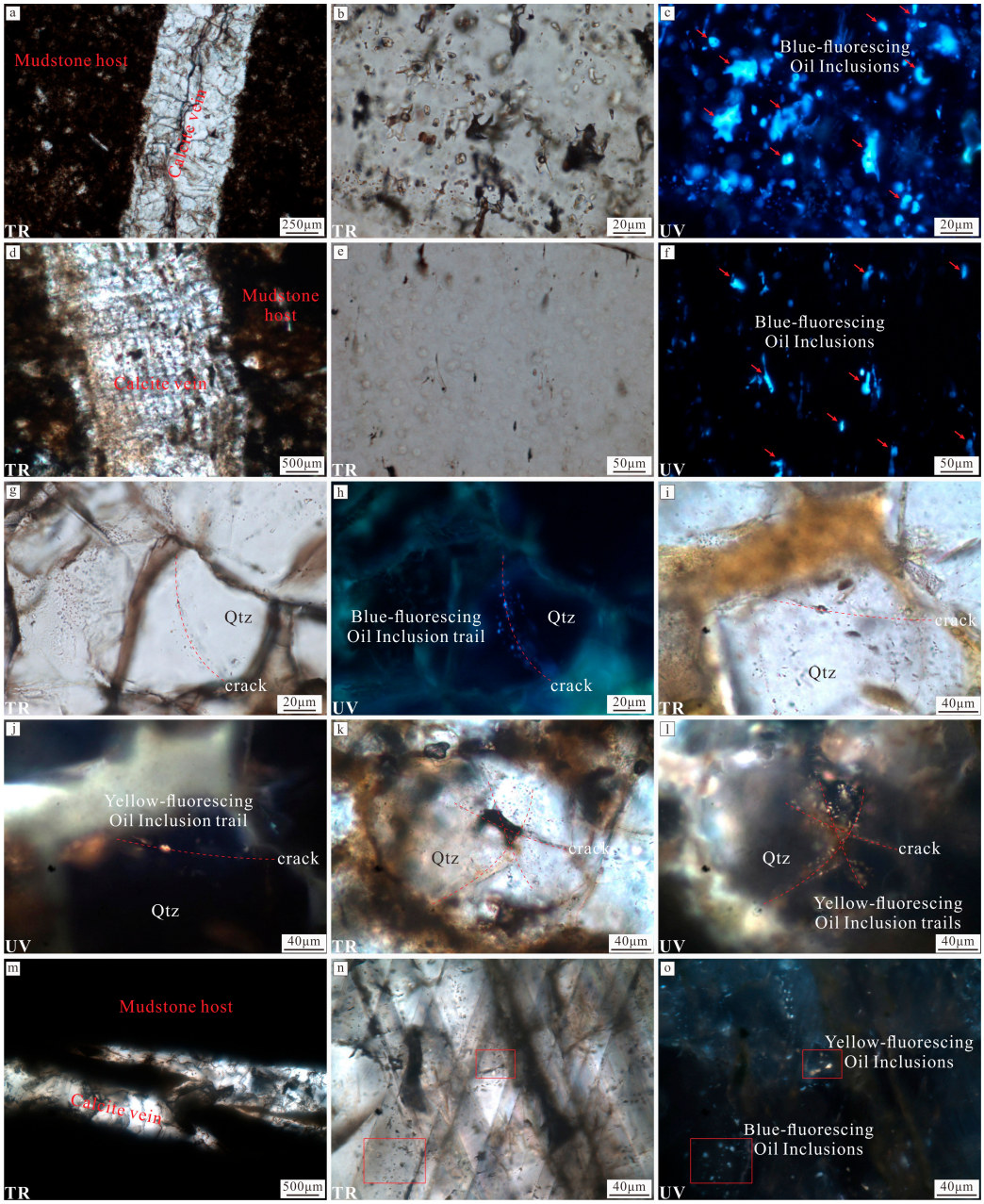


Figure 3. Occurrence of typical oil inclusions in samples. (**a**) Photomicrograph of the calcite vein hosted in mudstone, sample #14, well FSX1; (**b**,**c**) photomicrographs of the same field view under transmitted (TR) light and ultraviolet (UV) light showing blue-fluorescing oil inclusions trapped in the calcite vein in (**a**); (**d**) photomicrograph of the calcite vein hosted in mudstone, sample #13, well FSX1; (**e**,**f**) photomicrographs of the same field view under TR and UV lights showing blue-fluorescing oil inclusions trapped in the calcite vein in (**d**); (**g**,**h**) photomicrographs of the same field view under TR and UV lights showing a blue-fluorescing oil inclusions' trail along a crack through a quartz (Qtz) grain, sample #12, well FSX1; (**i**,**j**) photomicrographs of the same field view under TR and UV lights, showing a yellow-fluorescing oil inclusions' trail along a crack through a quartz (Qtz) grain, sample #3, well SX53; (**k**,**l**) photomicrographs of the same field view under TR and UV lights, showing a yellow-fluorescing oil inclusions' trail along a crack through a quartz (Qtz) grain, sample #1, well SX51; (**m**) photomicrograph of the calcite vein hosted in mudstone, sample #16, well H158; (**n**,**o**) photomicrographs of the same field view under TR and UV lights, showing blue- (the lower left red rectangle) and yellow-fluorescing (the central red rectangle) oil inclusions trapped in the calcite vein in (**m**).

4.2. Fluorescence Microspectroscopy

Fluorescence spectra of typical yellow-fluorescing and blue-fluorescing oil inclusions are illustrated in Figure 4a, and the quantified parameters of λ_{max} and $Q_{650/500}$ are listed in Table 1 and plotted in Figure 4b. According to the fluorescence colors of oil inclusions, their typical fluorescence spectra shapes, and the quantitative results, oil inclusions are classified into two types, including Kind A and Kind B. Kind A is of yellow-fluorescing oil inclusions (Figure 3j,l,o), including fluorescence spectra with a λ_{max} range of 541.8 nm to 579.1 nm (mean 552.9 nm) and a $Q_{650/500}$ range of 0.56 to 0.79 (mean 0.68), whereas Kind B is of blue-fluorescing oil inclusions (Figure 3c,f,h,o), including fluorescence spectra with a λ_{max} range of 487.5 nm to 523.3 nm (mean 505.8 nm) and a $Q_{650/500}$ range of 0.22 to 0.44 (mean 0.33) (Figure 4).

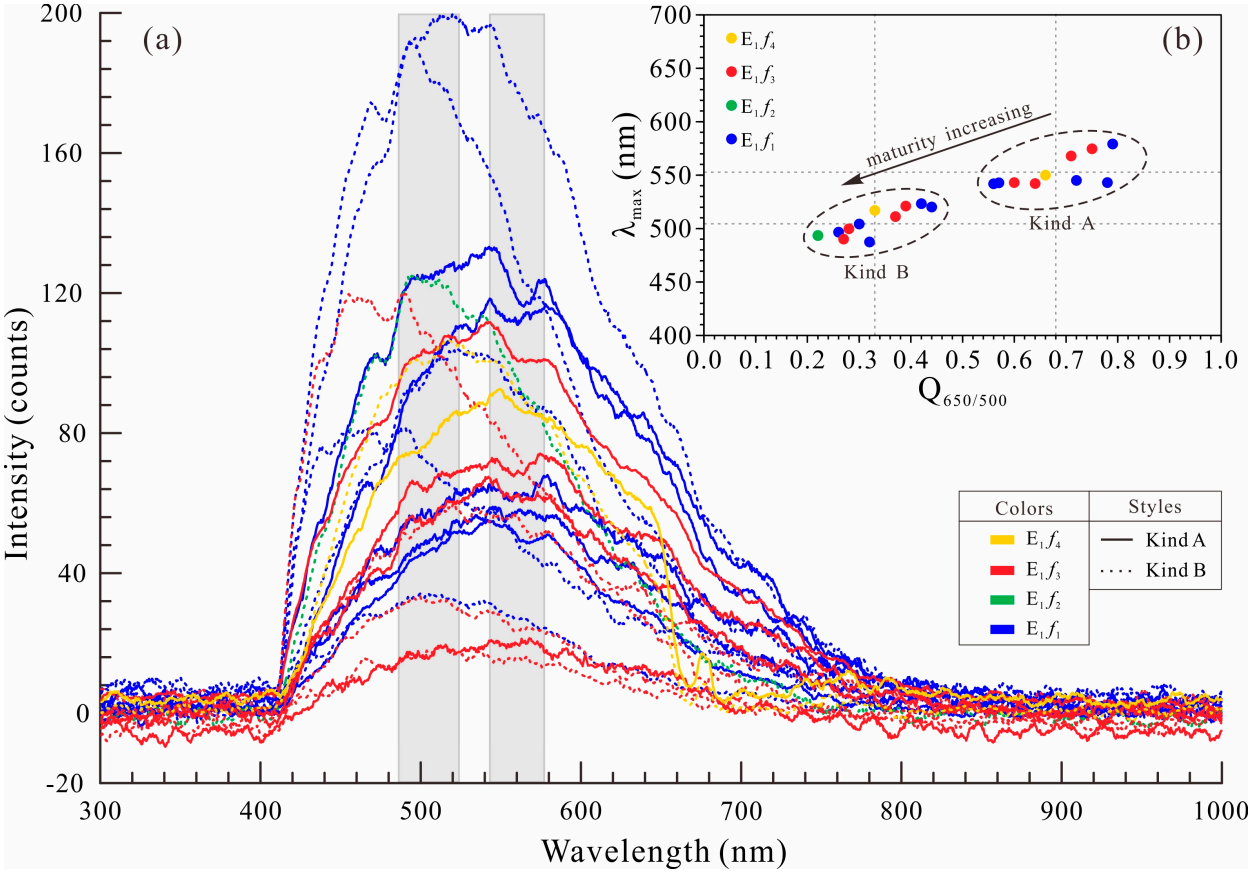


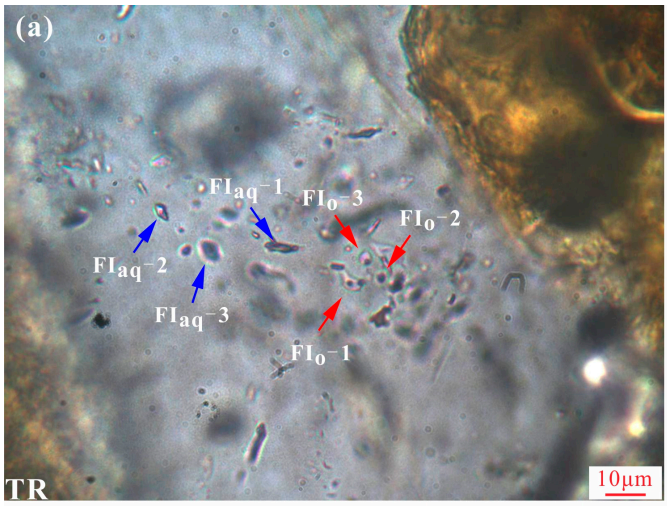
Figure 4. Fluorescence spectra (**a**) and λ_{max} versus $Q_{650/500}$ plot (**b**) of typical oil inclusions. The vertical gray bars in (**a**) illustrate the two λ_{max} ranges, and the dashed lines in (**b**) illustrate the mean values of the two λ_{max} ranges (horizontal) and the two $Q_{650/500}$ ranges (vertical).

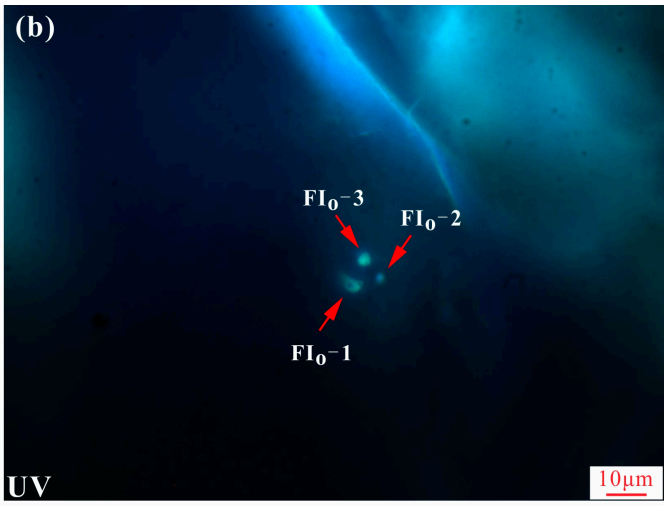
4.3. Microthermometry and Thermodynamic Modeling

The microthermometry results of typical oil inclusions and their coeval aqueous inclusions are listed in Table 1. It is suggested that typical oil inclusions of Kind A have a range in homogenization temperature between 62.6 °C and 101.9 °C, and typical oil inclusions of Kind B have a range in homogenization temperature between 88.7 °C and 129.1 °C. The homogenization temperature ranges of coeval aqueous inclusions for Kind A and Kind B are 72.6–111.9 °C and 98.5–139.1 °C, respectively.

Figure 5a,b show the coeval oil and aqueous inclusions that were used to reconstruct the trapping pressure in sample #3. The homogenization temperatures and bubble volumes (Figure 5c) were input to VTflinc software and gave the result of a *P-T* phase diagram (Figure 5d), which shows that the inclusions were trapped at a pressure of 276.92 Bar

(i.e., 27.692 MPa). In this research, forty-four paleopressures were extracted by thermodynamic modeling with fluid inclusions, as illustrated in Figure 6. The paleopressure in E_1f_1 is between 20.8 MPa (sample #4, well HX14) and 33.9 MPa (sample #14, well FSX1); the paleopressure in E_1f_2 is between 27.2 MPa and 28.6 MPa (sample #13, well FSX1); the paleopressure in E_1f_3 is between 23.3 MPa (sample #1, well SX51) and 32.9 MPa (sample #11, well FSX1); and the paleopressure in E_1f_4 is between 25.0MPa and 30.0 MPa (sample #16, well H158).





(c) Coeval inclusion data as input to VTFlinc

Inclusion type	Inclusion code	Fv (%)	Th (°C)	Mean Th (°C)	Mean Fv (%)
Aqueous	FI_{aq}-1	6	106.5	106.5	8
	FI_{aq}-2	8	104.8		
	FI_{aq}-3	10	108.2		
Oil	FI_{o}-1	10	94.4	95.6	10
	FI_{o}-2	11	96.8		
	FI_{o}-3	9	95.6		

Note: Fv-Filling volume of the bubble; Th-Homogenization temperature

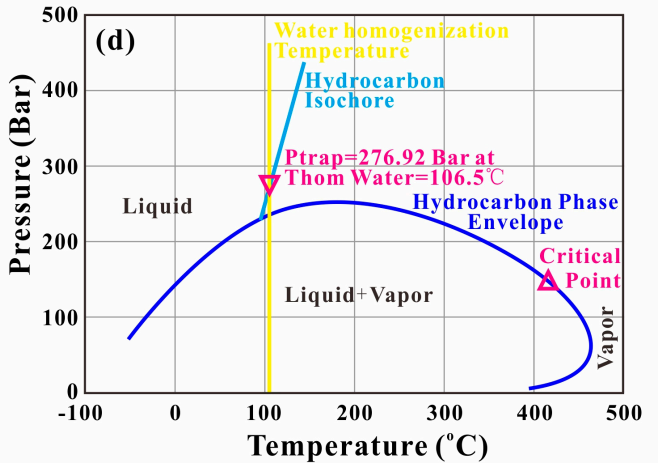


Figure 5. Demonstration of paleopressure acquired from sample #3, well SX53. (**a**) Oil and coeval aqueous inclusions under transmitted (TR) light; (**b**) the same field view as (**a**) under ultraviolet (UV) light; (**c**) arranged fluid inclusion data for the thermodynamic modeling; (**d**) *P-T* phase diagram of inclusion oils at the trapping point (Thom water-homogenization temperature of coeval aqueous inclusion, Ptrap trapping pressure of oil inclusion). The curves to the left and the right of the critical point are the bubble point curve and the dew point curve. Inside the hydrocarbon phase envelope is a two-phase region (liquid plus vapor), and outside is a single-phase region (liquid or vapor). Oil inclusion was trapped at a certain point (the trapping point was constrained by the water homogenization temperature) on the hydrocarbon isochore and evolved along it into the two-phase region (surface conditions).

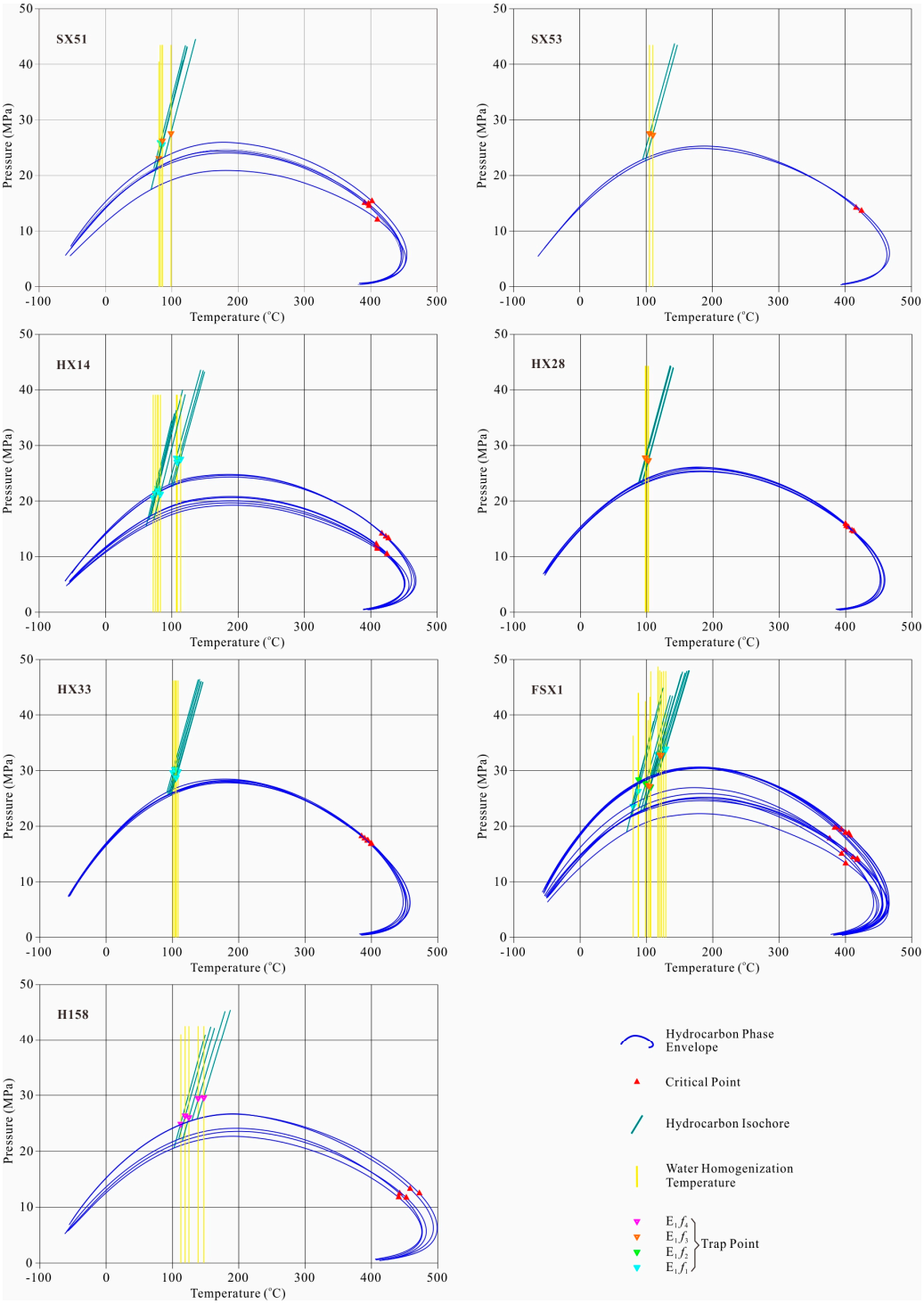


Figure 6. *P-T* phase diagrams of each typical oil inclusion showing the excavated paleopressures.

5. Discussion

5.1. Maturity Difference in Inclusion Oils

The fluorescence color of oil inclusions has been qualitatively used as a thermal maturity indicator of the migrating oils [26,28,31,32]. Researchers have also extensively discussed the relationship between fluorescence colors and the thermal maturity of oils [33–37]. According to the results of these discussions, the oil inclusions of Kind A have relatively lower maturity compared to the oil inclusions of Kind B in the Funing Formation of the Gaoyou Sag because there is a significant red shift in the λ_{max} and an obvious increase in $Q_{650/500}$ relative to Kind

B (Figure 4), which are hints of the maturity decreasing. Thus, it is suggested that Kind A and Kind B trapped oils of different maturities in different periods. The Funing Formation of the Gaoyou Sag experienced a history of multiple hydrocarbon charging periods.

5.2. Hydrocarbon Charging Periods

Oil inclusions are the original records of hydrocarbon activities in a sedimentary basin and have been widely used to reveal the history of hydrocarbon charging [38–43]. The operation details to determine hydrocarbon charging with the fluid inclusion technique have been elaborated in many studies [44–47]. By combining the homogenization temperature of coeval aqueous inclusions with the thermal evolution burial history curves, the trapping time of oil inclusions and the corresponding trapping depth can be readily acquired.

Figure 7 shows the determination results of trapping time and depth for oil inclusions entrapped in samples from well FSX1, from which we can see two obvious periods of hydrocarbon charging, especially illustrated by the data from the E_1f_1 (samples #14 and #15). Projecting all the trapping times from the seven wells on the same geological timescale shows that there are two episodes of hydrocarbon charging in the Funing Formation of the Gaoyou Sag (Figure 8). The first hydrocarbon charging (Episode 1) was only detected in well FSX1 and occurred between 52.8 Ma and 49.5 Ma, while the second hydrocarbon charging (Episode 2) was detected in all seven wells and happened between 47.0 Ma and 37.0 Ma. It seems that the two episodes are continuous hydrocarbon charging periods due to the short interval (2.5 Ma) between them, but they belong to two different charging periods according to the distinct characteristics of the two kinds of oil inclusions. Moreover, Episode 2 obviously had a longer duration than Episode 1, and it constitutes the main hydrocarbon charging period of the Funing Formation in the Gaoyou Sag.

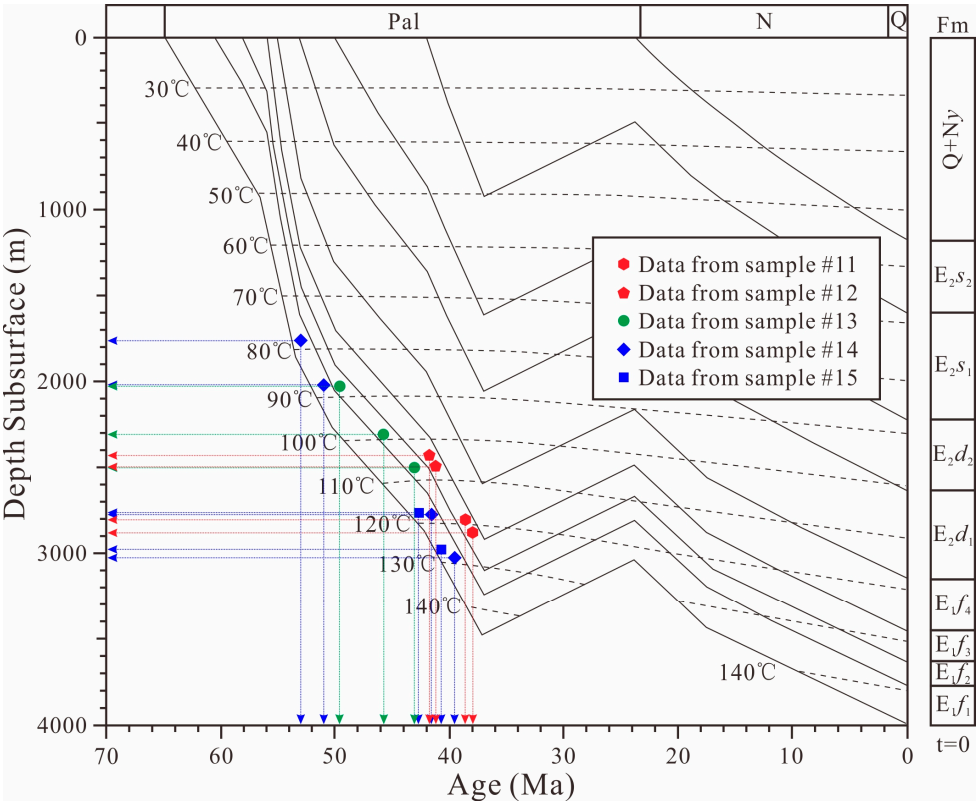


Figure 7. Determination of trapping time and depth of oil inclusions in samples from well FSX1. Solid black lines represent the burial history curves; dashed black lines represent the burial temperature of the reservoir. The colored horizontal dotted lines with arrows signify the trapping depth, while the colored vertical dotted lines with arrows mark the trapping time.

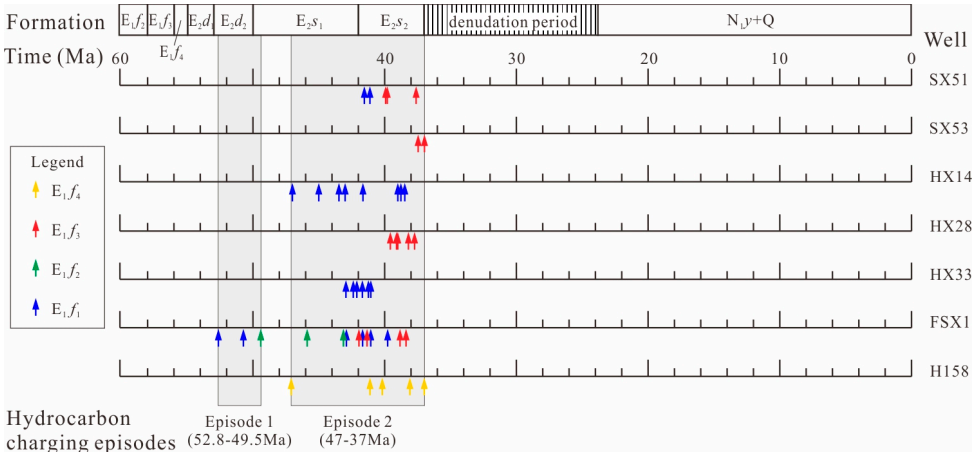


Figure 8. Hydrocarbon charging periods of the Funing Formation in the Gaoyou Sag.

5.3. Paleopressure and Its Evolution

Fluid inclusion is the original sample of paleofluid and recorded the temperature and pressure conditions while it was trapped. This is the reason that fluid inclusions can be used as geothermometers and geobarometers. Therefore, the trapping pressure can stand for the paleopressure of the formation.

A pressure coefficient (ratio of formation pressure to hydrostatic pressure) is usually used to characterize the state of pressure (underpressure, normal pressure, and overpressure). With the trapping pressure (paleopressure) and the trapping depth (paleo buried depth), which were used to calculate hydrostatic pressure, paleopressure coefficients were calculated and are illustrated in Figure 9. The paleopressure coefficient of Episode 1 can reach as high as 1.44, while that of Episode 2 can reach as high as 1.40. Obviously, all of Episode 1 and most of Episode 2 have paleopressure coefficients greater than 1.2, which suggests that these two periods of hydrocarbon charging are both characterized by abnormally high pressures (overpressure). Coupled with the trapping time and the present formation pressure coefficients, the evolution of paleopressure displays a process of rapid pressure increasing and decreasing and slow pressure increasing, and the evolution result is that the current pressure is not as high as what was reached during the hydrocarbon charging periods (Figure 9).

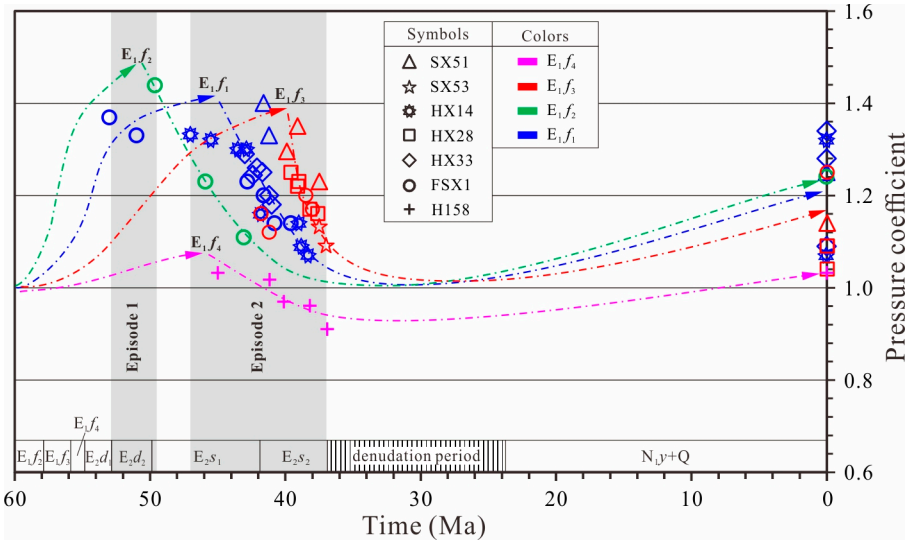


Figure 9. Paleopressure evolution of the Funing Formation in the Gaoyou Sag. Dashed lines with arrows illustrate the evolutionary trends in paleopressure.

Considering hydrocarbon generation as the origin of overpressure [48], the paleopressure reconstruction results suggest that the second member of the Funing Formation (E_1f_2) is obviously the center of abnormally high pressure. Overpressure in the first and third members of the Funing Formation (E_1f_1 and E_1f_3) is a kind of transfer overpressure due to the downward and upward expulsions of oils generated in E_1f_2. The abnormally high pressure in the E_1f_2 acted as the driving force for the primary migration of oils, and overpressures in E_1f_1 and E_1f_3 acted as the driving force for the secondary migration of oils. Figure 9 also indicates that the hydrocarbon activities in the fourth member of the Funing Formation (E_1f_4) occurred in a normal pressure system throughout the whole geological time.

As is commonly understood, current formation pressure has a significant impact on drilling engineering, and paleopressure plays an important role in the generation, migration, and accumulation of oil and gas. The reconstructed paleo-overpressure and the evolutionary process of the current pressure in the Funing Formation provide valuable references for determining the exploration direction of conventional clastic reservoirs in E_1f_1 and E_1f_3 in future work. Meanwhile, as pressure accumulated higher and higher in E_1f_1 and E_1f_3, the oil expulsion from E_1f_2 became harder and harder, which is beneficial for the enrichment of shale oils in E_1f_2. Hence, it is also helpful for understanding the enrichment mechanism of shale oils in the Funing Formation of the Gaoyou Sag.

6. Conclusions

Systematic fluid inclusion analysis suggested that yellow-fluorescing oil inclusions and blue-fluorescing oil inclusions were trapped during two episodes of hydrocarbon charging in the Funing Formation of the Gaoyou Sag. Episode 1 occurred from 52.8 Ma to 49.5 Ma, with the charging of lower maturity oils, and Episode 2 occurred from 47.0 Ma to 37.0 Ma, with the charging of higher maturity oils.

The reconstruction of paleopressure revealed that, during the hydrocarbon charging periods (both Episode 1 and Episode 2), the Funing Formation experienced abnormally high pressures. The E_1f_2 is the center of overpressure, from where the abnormally high pressures in the E_1f_1 and E_1f_3 were transferred. The paleopressure evolution in the Funing Formation of the Gaoyou Sag experienced a process of rapid pressure increasing and decreasing and then slow increasing.

Information established on hydrocarbon charging periods, paleopressures, and the evolutionary history in the Funing Formation through this study is meaningful for the future exploration and exploitation of conventional clastic reservoirs in the Gaoyou Sag and helpful for understanding the enrichment mechanism of shale oils in the Funing Formation as well.

Author Contributions: Conceptualization, C.L. and S.Q.; methodology, C.L. and Y.Z.; formal analysis, C.L.; investigation, Y.Z.; resources, S.Q.; writing—original draft preparation, C.L., S.Q. and Y.Z.; writing—review and editing, C.L.; supervision, S.Q. and Y.Z. All authors have read and agreed to the published version of the manuscript.

Funding: This study was financially supported by the Exploration and Development Research Institute of Jiangsu Oilfield Company, SINOPEC.

Data Availability Statement: Data will be available on request from the corresponding author.

Acknowledgments: We thank the two anonymous reviewers for their detailed reviews and helpful comments. All the tests were performed in the Key Laboratory of Tectonics and Petroleum Resources (China University of Geosciences), Ministry of Education. The authors give deep gratitude to them.

Conflicts of Interest: Authors Shiyou Qian and Yuancai Zheng are affiliated with the Company Exploration and Development Research Institute of Jiangsu Oilfield Company, SINOPEC. The remaining authors declare that the research was conducted in the absence of any commercial or financial relationships that could be construed as a potential conflict of interest.

References

1. Lee, M.K.; Williams, D.D. Paleohydrology of the Delaware Basin, western Texas: Overpressure development, hydrocarbon migration, and ore genesis. *AAPG Bull.* **2000**, *84*, 961–974.
2. Finkbeiner, T.; Zoback, M.; Flemings, P.; Stump, B. Stress, pore pressure, and dynamically constrained hydrocarbon columns in the South Eugene Island 330 field, northern Gulf of Mexico. *AAPG Bull.* **2001**, *85*, 1007–1031.
3. Nelson, P.H.; Gianoutsos, N.J.; Drake, R.M., II. Underpressure in Mesozoic and Paleozoic rock units in the Midcontinent of the United States. *AAPG Bull.* **2015**, *99*, 1861–1892. [CrossRef]
4. Su, A.; Chen, H.; Lei, M.; Li, Q.; Wang, C. Paleo-pressure evolution and its origin in the Pinghu slope belt of the Xihu Depression, East China Sea Basin. *Mar. Petrol. Geol.* **2019**, *107*, 198–213. [CrossRef]
5. Liu, Y.; Qiu, N.; Hu, W.; Li, H.; Shen, F.; Yao, Q. Temperature and pressure characteristics of Ordovician gas condensate reservoirs in the Tazhong area, Tarim Basin, northwestern China. *AAPG Bull.* **2019**, *103*, 1351–1381. [CrossRef]
6. Zeng, S.; Qiu, N.; Li, H.; Gao, J.; Long, K.; Jia, J.; Zhu, X. Generation and distribution of overpressure in ultra-deep carbonate reservoirs controlled by intra-cratonic strike-slip faults: The Ordovician of Shuntuoguole area in the Tarim Basin. *Mar. Petrol. Geol.* **2023**, *158*, 106515. [CrossRef]
7. Law, B.E.; Spencer, C.W. Abnormal pressures in hydrocarbon environments. In *Abnormal Pressures in Hydrocarbon Environments*; Memoir 70; Law, B.E., Ulmishek, G.F., Slavin, V.I., Eds.; AAPG: Tulsa, OK, USA, 1998; pp. 1–11.
8. Mann, D.M.; Mackenzie, A.S. Prediction of pore fluid pressure in sedimentary basins. *Mar. Petrol. Geol.* **1990**, *7*, 55–65. [CrossRef]
9. Zhang, J. Pore pressure prediction from well logs: Methods, modifications, and new approaches. *Earth-Sci. Rev.* **2011**, *108*, 50–63. [CrossRef]
10. Kong, L.; Chen, H.; Ping, H.; Zhai, P.; Liu, Y.; Zhu, J. Formation pressure modeling in the Baiyun Sag, northern South China Sea: Implications for petroleum exploration in deep-water areas. *Mar. Petrol. Geol.* **2018**, *97*, 154–168. [CrossRef]
11. Roedder, E.; Bodnar, R.J. Geologic pressure determinations from fluid inclusion studies. *Annu. Rev. Earth Planet. Sci.* **1980**, *8*, 263–301. [CrossRef]
12. Aplin, A.C.; Macleod, G.; Larter, S.R.; Pedersen, K.S.; Sorensen, H.; Booth, T. Combined use of Confocal Laser Scanning Microscopy and PVT simulation for estimating the composition and physical properties of petroleum in fluid inclusions. *Mar. Petrol. Geol.* **1999**, *16*, 97–110. [CrossRef]
13. Thiéry, R.; Pirononl, J.; Walgenwitz, F.; Montel, F. PIT (Petroleum Inclusion Thermodynamic): A new modeling tool for the characterization of hydrocarbon fluid inclusions from volumetric and microthermometric measurements. *J. Geochem. Explor.* **2000**, *69–70*, 701–704. [CrossRef]
14. Ping, H.; Thiéry, R.; Chen, H. Thermodynamic modeling of petroleum inclusions: The prediction of the saturation pressure of crude oils. *Geofluids* **2011**, *11*, 328–340. [CrossRef]
15. Aplin, A.C.; Larter, S.R.; Bigge, M.A.; Macleod, G.; Swarbrick, R.E.; Grunberger, D. Confocal microscopy of fluid inclusions reveals fluid-pressure histories of sediments and an unexpected origin of gas condensate. *Geology* **2000**, *28*, 1047–1050. [CrossRef]
16. Chen, H.; Yao, S.; Wang, J.; Li, C. Thermodynamic modeling of fluid-bearing natural gas inclusions for geothermometer and geobarometer of overpressured environments in Qiongdongnan Basin, South China Sea. *J. China Univ. Geosci.* **2002**, *13*, 240–247.
17. Munz, I.A.; Wangen, M.; Girard, J.P.; Lacharpagne, J.C.; Johansen, H. Pressure–temperature–time–composition (P–T–t–X) constraints of multiple petroleum charges in the Hild field, Norwegian North Sea. *Mar. Petrol. Geol.* **2004**, *21*, 1043–1060. [CrossRef]
18. Chen, L. Estimation of the amount of erosion at unconformities in the late stage of the Eocene Sanduo period in the Subei Basin, China. *Pet. Sci.* **2009**, *6*, 383–388. [CrossRef]
19. Liu, Y.; Chen, Q.; Wang, X.; Hu, K.; Cao, S.; Wu, L.; Gao, F. Influence of normal fault growth and linkage on the evolution of a rift basin: A case from the Gaoyou depression of the Subei Basin, eastern China. *AAPG Bull.* **2017**, *101*, 265–288. [CrossRef]
20. Gao, G.; Yang, S.; Zhang, W.; Wang, Y.; Gang, W.; Lou, G. Organic geochemistry of the lacustrine shales from the Cretaceous Taizhou Formation in the Gaoyou Sag, Northern Jiangsu Basin. *Mar. Petrol. Geol.* **2018**, *89*, 594–603. [CrossRef]
21. Su, P.; Hu, S.; Li, S.; Song, Y. Hydrocarbon generation kinetics of salinized lacustrine source rocks in the upper Cretaceous-Paleocene South Yellow Sea Basin, offshore eastern China. *Geoenergy Sci. Eng.* **2023**, *227*, 211888. [CrossRef]
22. Zhang, X.; Lin, C.M.; Yin, Y.; Zhang, N.; Zhou, J.; Liu, Y.R. Sedimentary characteristics and processes of the Paleogene Dainan Formation in the Gaoyou Depression, North Jiangsu Basin, eastern China. *Pet. Sci.* **2016**, *13*, 385–401. [CrossRef]
23. Liu, X.; Lai, J.; Fan, X.; Shu, H.; Wang, G.; Ma, X.; Liu, M.; Guan, M.; Luo, Y. Insights in the pore structure, fluid mobility and oiliness in oil shales of Paleogene Funing Formation in Subei Basin, China. *Mar. Petrol. Geol.* **2020**, *114*, 104228. [CrossRef]
24. Liu, C.; Xie, Q.; Wang, G.; Zhang, C.; Wang, L.; Qi, K. Reservoir properties and controlling factors of contact metamorphic zones of the diabase in the northern slope of the Gaoyou Sag, Subei Basin, eastern China. *J. Nat. Gas Sci. Eng.* **2016**, *35*, 392–411. [CrossRef]
25. Munz, I.A. Petroleum inclusions in sedimentary basins: Systematics, analytical methods and applications. *Lithos* **2001**, *55*, 195–212. [CrossRef]
26. Goldstein, R.H.; Reynolds, T.J. *Systematics of Fluid Inclusions in Diagenetic Minerals*; Short Course 31; SEPM: Tulsa, OK, USA, 1994; 199p.
27. Chi, G.; Diamond, L.W.; Lu, H.; Lai, J.; Chu, H. Common problems and pitfalls in fluid inclusion study: A review and discussion. *Minerals* **2021**, *11*, 7. [CrossRef]
28. Stasiuk, L.D.; Snowdon, L.R. Fluorescence micro-spectrometry of synthetic and natural hydrocarbon fluid inclusions: Crude oil chemistry, density and application to petroleum migration. *Appl. Geochem.* **1997**, *12*, 229–241. [CrossRef]

29. Goldstein, R.H. Fluid inclusions in sedimentary and diagenetic systems. *Lithos* **2001**, *55*, 159–193. [CrossRef]
30. Swarbrick, R.E.; Osborne, M.J.; Grunberger, D.; Yardley, G.S.; Macleod, G.; Aplin, A.C.; Larter, S.R.; Knight, I.; Auld, H.A. Integrated study of the Judy Field (Block 30/7a)—An overpressured Central North Sea oil/gas field. *Mar. Petrol. Geol.* **2000**, *17*, 993–1010. [CrossRef]
31. McLimans, R.K. The application of fluid inclusions to migration of oil and diagenesis in petroleum reservoirs. *Appl. Geochem.* **1987**, *2*, 585–603. [CrossRef]
32. Guilhaumou, N.; Szydlowskii, N.; Pradier, B. Characterization of hydrocarbon fluid inclusions by infra-red and fluorescence microspectrometry. *Mineral. Mag.* **1990**, *54*, 311–324. [CrossRef]
33. George, S.C.; Ruble, T.E.; Dutkiewicz, A.; Eadington, P.J. Assessing the maturity of oil trapped in fluid inclusions using molecular geochemistry data and visually-determined fluorescence colours. *Appl. Geochem.* **2001**, *16*, 451–473. [CrossRef]
34. Oxtoby, N.H. Comments on: Assessing the maturity of oil trapped in fluid inclusions using molecular geochemistry data and visually-determined fluorescence colours. *Appl. Geochem.* **2002**, *17*, 1371–1374. [CrossRef]
35. George, S.C.; Ruble, T.E.; Dutkiewicz, A.; Eadington, P.J. Reply to comment by Oxtoby on "Assessing the maturity of oil trapped in fluid inclusions using molecular geochemistry data and visually-determined fluorescence colours". *Appl. Geochem.* **2002**, *17*, 1375–1378. [CrossRef]
36. Ping, H.; Chen, H.; George, S.C.; Li, C.; Hu, S. Relationship between the fluorescence color of oil inclusions and thermal maturity in the Dongying Depression, Bohai Bay Basin, China: Part 1. Fluorescence evolution of oil in the context of hydrous pyrolysis with increasing maturity. *Mar. Petrol. Geol.* **2019**, *100*, 1–19. [CrossRef]
37. Ping, H.; Chen, H.; George, S.C.; Li, C.; Hu, S. Relationship between the fluorescence colour of oil inclusions and thermal maturity in the Dongying Depression, Bohai Bay Basin, China: Part 2. fluorescence evolution of oil in the context of petroleum generation, expulsion and cracking under geological conditions. *Mar. Petrol. Geol.* **2019**, *103*, 306–319.
38. Parnell, J.; Carey, P.; Duncan, W. History of hydrocarbon charge on the Atlantic margin: Evidence from fluid-inclusion studies, West of Shetland. *Geology* **1998**, *26*, 807–810. [CrossRef]
39. Parnell, J.; Middleton, D.; Chen, H.; Hall, D. The use of integrated fluid inclusion studies in constraining oil charge history and reservoir compartmentation: Examples from the Jeanne d'Arc Basin, offshore Newfoundland. *Mar. Petrol. Geol.* **2001**, *18*, 535–549. [CrossRef]
40. Liu, K.; Eadington, P. Quantitative fluorescence techniques for detecting residual oils and reconstructing hydrocarbon charge history. *Org. Geochem.* **2005**, *36*, 1023–1036. [CrossRef]
41. Gong, S.; George, S.C.; Volk, H.; Liu, K.; Peng, P. Petroleum charge history in the Lunnan Low Uplift, Tarim Basin, China—Evidence from oil-bearing fluid inclusions. *Org. Geochem.* **2007**, *38*, 1341–1355. [CrossRef]
42. Atwah, I.; Mohammadi, S.; Moldowan, J.M.; Dahl, J. Episodic hydrocarbon charge in tight Mississippian reservoirs of Central Oklahoma, USA: Insights from oil inclusion geochemistry. *Mar. Petrol. Geol.* **2021**, *123*, 104742. [CrossRef]
43. Volk, H.; George, S.C. Using petroleum inclusions to trace petroleum systems—A review. *Org. Geochem.* **2019**, *129*, 99–123. [CrossRef]
44. Cao, J.; Jin, Z.; Hu, W.; Zhang, Y.; Yao, S.; Wang, X.; Zhang, Y.; Tang, Y. Improved understanding of petroleum migration history in the Hongche fault zone, northwestern Junggar Basin (northwest China): Constrained by vein-calcite fluid inclusions and trace elements. *Mar. Petrol. Geol.* **2010**, *27*, 61–68. [CrossRef]
45. Li, C.; Chen, H. Hydrocarbon inclusion characteristics in the Cambrian-Ordovician carbonates of the TS2 well: Implication for deep hydrocarbon exploration in the Tahe oilfield, Tarim Basin, northwest China. *Acta Geol. Sin. (Engl. Ed.)* **2015**, *89*, 852–860.
46. Zhao, X.; Zhang, L.; Jin, F.; Wang, Q.; Bai, G.; Li, Z.; Wang, J. Hydrocarbon charging and accumulation history in the Niudong buried hill field in the Baxian Depression, eastern China. *Mar. Petrol. Geol.* **2017**, *88*, 343–358. [CrossRef]
47. Li, C.; Chen, H.; Liu, H. Fluid inclusion constrained multiple petroleum chargings in the lithologic reservoirs of the late Eocene Shahejie Formation in the Minfeng Sag, Bohai Bay Basin, east China. *Energies* **2022**, *15*, 3682. [CrossRef]
48. Zheng, Y.; Wu, Y. Forming mechanism and distribution characteristics of overpressure in the first member of Funing Formation in Sha–Hua–Wa area of Gaoyou Sag. *Complex Hydrocarb. Reserv.* **2016**, *9*, 1–5. (In Chinese)

Disclaimer/Publisher's Note: The statements, opinions and data contained in all publications are solely those of the individual author(s) and contributor(s) and not of MDPI and/or the editor(s). MDPI and/or the editor(s) disclaim responsibility for any injury to people or property resulting from any ideas, methods, instructions or products referred to in the content.